analytical chemistry

Article

pubs.acs.org/ac

Nanometer Scale Scanning Electrochemical Microscopy Instrumentation

Jiyeon Kim,[†,○] Christophe Renault,[‡,○] Nikoloz Nioradze,[§] Netzahualcóyotl Arroyo-Currás,[∥] Kevin C. Leonard,[*,⊥] and Allen J. Bard[*,#]

[†]Department of Chemistry, The University of Rhode Island, Kingston, Rhode Island 02881, United States

[‡]Laboratoire de Physique de la Matière Condensée, Ecole Polytechnique Palaiseau, 91128 Palaiseau, France

[§]The Institute of Inorganic Chemistry and Electrochemistry, Tbilisi State University, Tbilisi 0179, Georgia

[∥]Department of Chemistry and Biochemistry, University of California Santa Barbara, Santa Barbara, California 93111, United States

[⊥]Center for Environmentally Beneficial Catalysis, Department of Chemical and Petroleum Engineering, The University of Kansas, Lawrence, Kansas 66047, United States

[#]Center for Electrochemistry, Department of Chemistry, The University of Texas at Austin, Austin, Texas 78712, United States

Supporting Information

ABSTRACT: We report the crucial components required to perform scanning electrochemical microscopy (SECM) with nanometer-scale resolution. The construction and modification of the software and hardware instrumentation for nanoscale SECM are explicitly explained including (1) the LabVIEW code that synchronizes the SECM tip movement with the electrochemical response, (2) the construction of an isothermal chamber to stabilize the nanometer scale gap between the tip and substrate, (3) the modification of a commercial bipotentiostat to avoid electrochemical tip damage during SECM experiments, and (4) the construction of an SECM stage to avoid artifacts in SECM images. These findings enabled us to successfully build a nanoscale SECM, which can be utilized to map the electrocatalytic activity of individual nanoparticles in a typical ensemble sample and study the structure/reactivity relationship of single nanostructures.

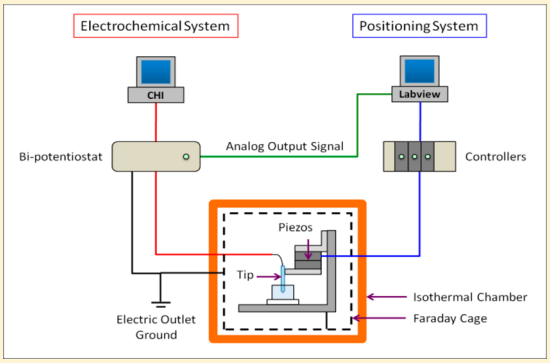

Scanning electrochemical microscopy (SECM) is a scanning-probe technique that can provide reactivity as well as topographic information, especially in the solution phase. A small electrode tip is used as an SECM probe, which is raster scanned across a substrate surface, typically with a small tip/substrate distance. Since SECM is not an optical technique, it does not need high activation energies or irradiation, thus is free from diffraction limits. Conventional SECM studies with spatial resolutions at the micrometer scale have evolved through pioneering studies by Amemiya, Mirkin, and our group and have showed that nanometer resolution is feasible.[1,2] Certainly, other hybrid types of SECM techniques for the nanoscale such as atomic force microscopy (AFM),[3−5] scanning tunneling microscopy,[6] impedance,[7−10] shear force,[11−14] scanning ion conductance microscopy,[15−17] scanning electrochemical cell microscopy,[18] and voltage-switching mode SECM[19] have also been demonstrated by various groups.

However, this nontrivial imaging at the nanometer level demands a number of new factors be considered. The tip size and its distance from the surface are the determining factors for the overall resolution. Nanometer-size tips are brittle and susceptible to damage by electrostatic discharge (ESD)[20] and vibrations. They are also easily contaminated; thereby, extremely high purity solutions are crucial.[21] Positioning and maintaining the tip at nanometer distances needs a high level of tip positional stability.[22] This is because the tip in SECM never directly contacts the surface, contrary to other scanning probe techniques (e.g., atomic force microscopy). Thereby, fine control of the tip position and the thermal stability of the system is required. The nanoscale SECM that we demonstrate here not only focuses on improving the resolution of the image but also on improving the tip positioning capability over the target at the tens of nanometer level without direct contact. The latter capability enables the measurement of extremely fast kinetics with highly enhanced mass transfer rates. To achieve such a high spatial resolution and high positional stability in the z direction, as well as lateral resolution for imaging, there are two crucial requirements: (1) suppressing thermal drift and (2) preventing potentiostat-induced tip damage at nanoscale distances. In that sense, we report the crucial components required to perform SECM with nanometer-scale resolution. In the following sections we explain the construction and the modification of the software and

Received: August 4, 2016
Accepted: September 23, 2016
Published: September 23, 2016

DOI: 10.1021/acs.analchem.6b03024
Anal. Chem. 2016, 88, 10284−10289

instrumentation hardware for the nanoscale SECM, including (1) the LabVIEW code developed to synchronize the SECM tip movement with electrochemical response, (2) the construction of an isothermal chamber to stabilize the nanometer-scale gap between the tip and substrate, (3) the modification of a commercial bipotentiostat to avoid electrochemical tip damage during SECM experiments, and (4) the construction of an SECM stage to avoid artifacts in SECM images.

EXPERIMENTAL SECTION

A CHI760E bipotentiostat (CH Instrument, Austin, TX) was used for electrochemical control. All relay switches of the bipotentiostat were physically removed to avoid electrochemical damage of nanometer-sized Pt nanoelectrodes during SECM. For the electrochemistry, a four electrode cell configuration was used with two Pt wires as quasi reference (QRE) and counter electrodes. The electrochemistry was operated with the CHI software. Simultaneously, the piezo was operated by the LabVIEW code, which also read the analog output signal (current) from the CHI760E bipotentiostat through a data acquisition board (USB-6009 Multifunction I/O, National Instrument). This synchronized the movement of the piezoelectric actuators with the corresponding tip current as a function of distance between the nano tip and the substrate.

Details on approaching the SECM tip to within the feedback distance (~one tip radius) are provided in the Supporting Information. After the SECM tip was positioned close to the substrate, the constant-height SECM images were obtained at 200 nm/s (incremental distance 20 nm per incremental time 0.1 s). To get the constant-height SECM image based on H^+ reduction/H_2 oxidation, −1.0 V and −0.4 V vs Pt QRE were applied to the nanotip and Pt nanoparticles (NPs) on highly oriented pyrolytic graphite (HOPG), respectively, where H^+ was reduced at the nanotip and tip generated H_2 was oxidized at the Pt NPs on HOPG substrate. Other SECM images were obtained in an electrolyte solution containing 1 mM ferrocenyl methyl trimethylammonium ($FcTMA^+$), 10 mM $NaClO_4$, where 0.3 V and −0.1 V vs Pt QRE were applied to the nanotip and Pt NP/HOPG substrate, respectively. Here, $FcTMA^+$ was oxidized at the nanotip and tip generated $FcTMA^{2+}$ was reduced at the substrate with diffusion controlled rates. All experiments were carried out in the isothermal chamber at a relative humidity maintained over 30% at 22 °C with ESD protection.[20]

SOFTWARE: LABVIEW CODE

The instrument has a bipotentiostat and a stage equipped with piezoelectric actuators operated with custom-software. National Instruments' LabVIEW was used to create the software to interface and synchronize the tip motion with the measured tip current from the bipotentiostat, similar to what Leonard and coworkers previously reported.[23] Figure S1 in the Supporting Information shows a schematic of the LabVIEW block diagram used to code the SECM mapping technique. The data acquisition of the analog output signal from the bipotentiostat (top section of Figure S1) and the motion-control of the piezos (bottom section of Figure S1) were performed in parallel using a nested for-loop architecture. The nested for-loop structure allows for the tip to be raster-scanned across the substrate. The interior for-loop steps the piezo in the *x*-direction for a set number of steps, and upon completion of the interior for-loop, the piezo performs one step in the *y*-direction and moves the piezo back to the initial *x* position. All custom subVIs that control the motion of the piezos internally call the Physik Instrumente's LabVIEW driver, and the data acquisition device was set to measure the analog input (AI) signal using National Instruments' DAQmx driver. An advantage of developing our own custom subVIs, combined with the modularity of LabVIEW, is that it allows for different motion-control manufacturers to be utilized, if necessary, by simply changing which LabVIEW driver is called inside this custom subVIs. Additional details and LabVIEW sample code are provided in the Supporting Information.

We intentionally separated the tip positioning control system from the electrochemistry using two different circuits as shown in the diagram in Figure 1 to avoid any possible conflicts between

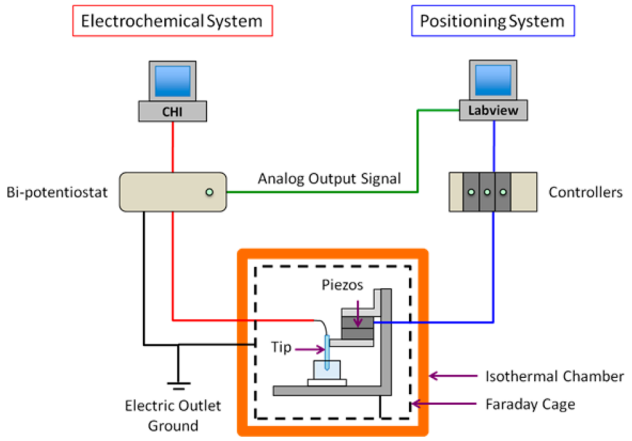

Figure 1. Schematic diagram of nanometer scale SECM (the scheme shown here is used in our previous work.[24] Copyright 2016 American Chemical Society).

the two different softwares. Here, the first computer operates the bipotentiostat (left computer in Figure 1) while on a second computer (on the right in Figure 1), the custom-developed LabVIEW program controls the movement of the piezos and synchronizes their movement with the tip current by reading the analog output signal from the bipotentiostat through a data acquisition board. We use a single ground to avoid any ground loop issues. All the conducting parts in the isothermal chamber and the electronic equipment are grounded to protect the SECM tip electrode from electrostatic discharge (ESD) damage.[20]

HARDWARE FOR VERTICAL AND LATERAL SPATIAL RESOLUTIONS AT NANOMETER SCALE

Isothermal Chamber: Stable Nanogap in SECM. To achieve a stable nanometer gap between the tip and the substrate during SECM measurements, two major components are required, (1) a highly precise piezo and (2) an isothermal chamber to suppress the thermal drift.[22] First, we used the XYZ piezo stage comprising an XY piezo (P620.2CL, Physik Instrumente) and a Z piezo (P620.ZCL, Physik Instrumente) bolted together. These piezos have a capacitive sensor placed inside each stage, enabling control of their motion with a resolution of 0.2 nm (in closed-loop), thus making them suitable for nanoscale SECM. The position of the piezo set by the operator is kept constant within only ±1 nm under our experimental conditions. PIMikroMove (PI) was used to control the drift compensation mode (DCO) to eliminate drift in the digital-analog converters on the E-816 submodule plugged into the main board of the controller.

DOI: 10.1021/acs.analchem.6b03024
Anal. Chem. 2016, 88, 10284−10289

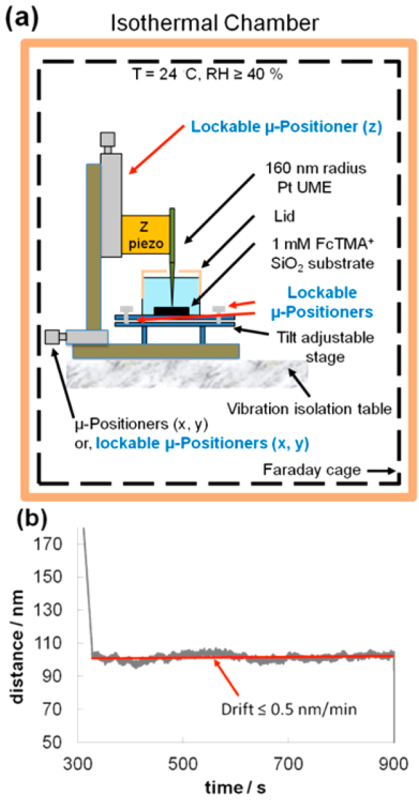

Figure 2. (a) Schematic representations of a SECM stage placed in the isothermal chamber. (b) Distance−time curves obtained with a 160 nm radius Pt tip and SiO_2 substrate in 1 mM FcTMA+ solution using SECM instruments shown in panel a. The resulting tip position in the *z*-axis drifted less than 0.5 nm/min.

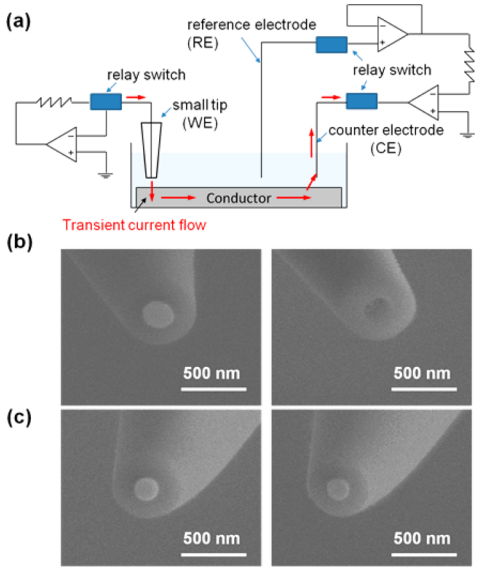

Figure 3. (a) Possible flow of the transient current from a working-electrode amplifier to a Pt tip, to a conductive substrate, and finally to a counter electrode. Red arrows depict transient current flow. (b, c) SEM images of Pt tip before (left) and after (right) SECM experiment where the tip−substrate potential difference is 400 mV or 150 mV, respectively. Only the right image in panel b shows distinct damage on the Pt surface with a scratched shape by electrochemical etching.

The maximum travel distance of the piezos is 50 μm. Each piezo is connected to a controller (E-621.CR, Physik Instrumente). The controllers are placed in an E-501.621 (Physik Instrumente) chassis. A single USB cable is used to interface the controllers with a computer, thus the LabVIEW

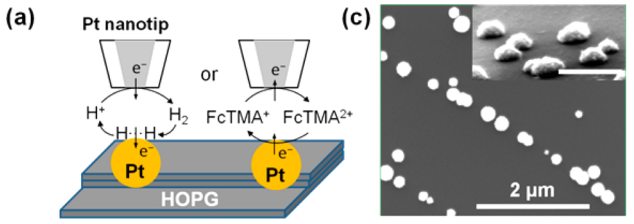

Figure 4. (a) Schematic view of electron transfer (ET) reactions occurring at Pt NPs in the presence of H^+ (left) or $FcTMA^+$ (right). (b) FE-SEM images of electrodeposited Pt NPs on HOPG. The inset shows a side view with a 500 nm scale bar. Mostly, Pt NPs are along the edge of HOPG. (Data shown here are used in our following work.[24] Copyright 2016 American Chemical Society).

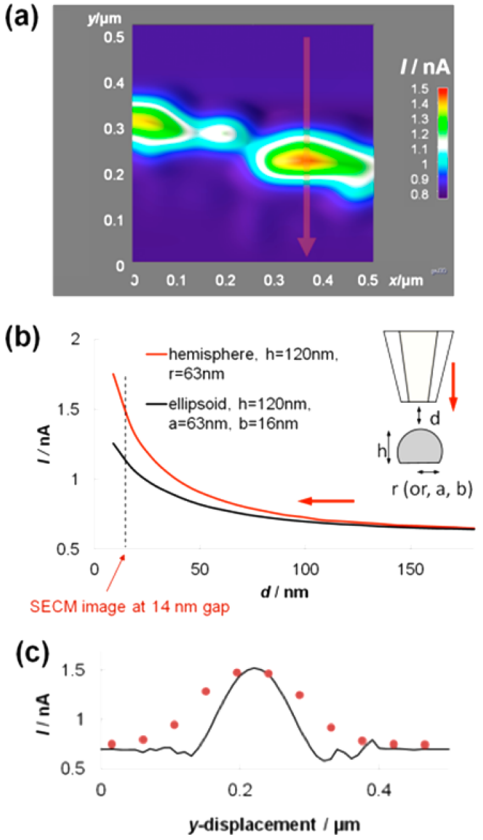

Figure 5. (a) SECM image of the hydrogen oxidation reaction at Pt NPs with $E_{tip} = -1.0$ V, $E_{substrate} = -0.4$ V vs Pt QRE in 2 mM $HClO_4$, 10 mM $NaClO_4$. The tip scan rate is 200 nm/s. (b) Theoretical tip current−distance curves for an inlaid-disk tip with RG 2.5 approaching either a reactive ellipsoidal or hemispherical to spherical NP with height (h), long axis radius (a), short axis radius (b), or radius (r) on an inert substrate. d denotes the gap between the tip and the highest point of the NP. The SECM image in panel a was obtained at 14 nm over an apex of a NP, thus 134 nm over the HOPG surface (detailed information can be found in ref 24). (c) Cross-sectional current responses along the red arrow from the SECM image in panel a. The maximum current magnitude in experimental curves (solid lines) agreed well with that in theoretical simulation (circles). In this analysis, the ET reaction at Pt NPs is controlled by diffusion. A discrepancy, however, exists in current peak width. (Data shown here are used in our previous work.[24] Copyright 2016 American Chemical Society).

DOI: 10.1021/acs.analchem.6b03024
Anal. Chem. 2016, 88, 10284−10289

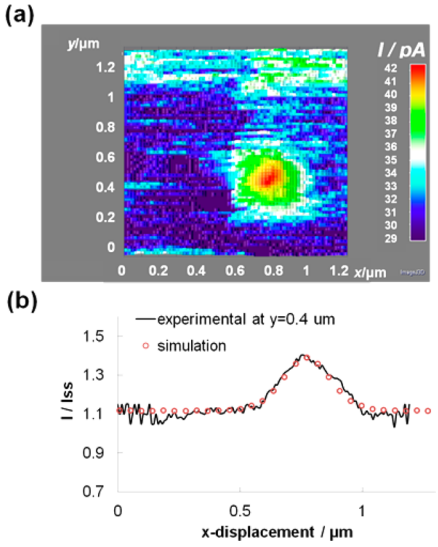

Figure 6. (a) SECM image of an individual Pt NP obtained in 1 mM $FcTMA^+$, 10 mM $NaClO_4$ with E_{tip} = 0.3 V, $E_{substrate}$ = −0.1 V vs Pt QRE after replacing both *x*- and *y*-unlockable micropositioners with lockable micropositioners. The Pt UME was scanned at 200 nm/s (20 nm incremental distance per 0.1 s incremental time). (b) Cross-sectional current responses along y = 0.4 μm from the SECM image in panel a. The experimental curves (solid lines) fit well with theoretical simulation (circles) in terms of current magnitudes, where the electron transfer reaction at Pt NPs is governed by diffusion control in this analysis. A good agreement between two data sets is seen in current peak width proving the image is from a single NP. (Data shown here are used in our previous work.[24] Copyright 2016 American Chemical Society).

program allows controlling the position of the piezos (detailed description of the LabVIEW program is provided in the Supporting Information). The XYZ piezo stage is mounted on the SECM stage (linear stage series 600, Newport), where the manual micropositioners are also mounted for long-distance translocations (<2.5 cm) in the *x*, *y* and *z*-axes. Specifically, a lockable differential micropositioner (lockable differential micropositioner DM-25L, Newport) is used in the *z*-axis. The lockable micropositioner minimizes the physical creeping or drift in the SECM system once they are locked, thus ensuring good stability of the stage. Because of this, the tilt adjustable substrate stage is also made with three lockable differential micropositioners (lockable differential micropositioner DM-13L, Newport) at the triangular positions (Figure 2a).

The constructed SECM stages are placed in an isothermal chamber, where the thermal drift is suppressed as reported elsewhere.[22] In this work, we constructed an isothermal chamber made with polystyrene foam (Lightweight Polystyrene Foam Insulation, 48 in.× 48 in. × 2 in., high density, 9255K3, McMaster Carr), where a vibration isolation table made with stainless steel acts as a heat sink (Figure 2a, detailed information is in the Supporting Information).

The stabilized gap between the tip and the substrate was experimentally confirmed by approaching the tip over the substrate, then stopping the tip approach at a distance comparable to the tip radius and monitoring the tip current over time in 1 mM $FcTMA^+$ solution as shown in Figure 2b. A Pt tip with a 160 nm radius was held at 100 nm above the insulating SiO_2 substrate, and the tip current, which is sensitive to a change in distance between the tip and the substrate, was monitored over time. In Figure 2b, the resulting distance-time curve was converted from the current−time curve. The monotonic tip drift level in the *z*-direction was less than 0.5 nm/min reflecting stabilized temperature in the chamber, which is stable enough to get the high-quality SECM images as well as quantitative SECM measurements (more detailed information about the current fluctuation is in the Supporting Information.)

Removal of Biopotentiostat Relay Switches: Suppressing Electrochemical Damages of Nanotips. We modified our commercially available bipotentiostat (CHI760E, CH Instrument, Austin, TX) to avoid electrochemical damage to the nanometer-size tip during SECM experiments, especially where a tip is positioned near a conductive substrate. In our SECM measurement, the "cell on between runs" function is active to keep the relay switches turned on between measurements.[20] However, the switches are transiently turned off for a very short time at the beginning and end of a measurement, which may saturate the amplifiers for a very short time, thus the amplifier transiently experiences a high output voltage. Subsequently, the high output voltage in the amplifiers drives the charging of the tip. A tip ≤200 nm in diameter can be sufficiently charged up during this short time, whereas this time is too short for a larger tip (∼1 μm). In this case, transient currents can flow if a current pathway is provided. Specifically, this process is facilitated when the tip is positioned near the conductive substrate because discharging current can flow through the conductive substrate within the nanometer sized gap between tip and the substrate rather than through the bulk solution, thereby electrochemically etching the tip (red arrows depict the transient current flow in Figure 3a). This discharging process can occur either from the working electrode amplifier to the tip and then to the substrate or from the counter electrode amplifier to the substrate and then to the tip. Accordingly, the substrate potential with respect to the tip potential could become an issue. In fact, we observed that tip damage depends on the substrate potential, thus more damage on the tip was seen at larger tip−substrate potential differences as shown in Figure 3b,c. Such tip damage can happen readily, unknowingly, and repetitively during the SECM experiment.

On the basis of the above-speculated mechanism, we expect that the saturation does not occur if the switches are removed and the electrodes are permanently connected to the amplifier. Accordingly, we removed all relay switches for working electrode 1 (WE1), working electrode 2 (WE2), counter electrode (CE), and reference electrode (RE) from our bipotentiostat by following the manufacturer's instructions (Figure S4). After removal, we shorted the connections between "common" and "normal open" in relay switches, thus the circuit is always closed without transient disconnection. We confirmed the intactness of the Pt tip by scanning electron microscopy after the SECM experiments with a relay-switch-removed bipotentiostat (Figure S5 in the Supporting Information).

Physically Stable Tip Positioners: Artifact of NP Shapes in the SECM Image and Its Suppression. We discovered that artifacts might arise in SECM images due to instrumental defects. As schematically shown in Figure 4a, SECM was employed with an inlaid Pt nanotip to study individual Pt NPs electrodeposited on HOPG, (Figure 4b) by mapping electrochemical reactions at their surface. The FIB-milled Pt nanotip used for SECM imaging has a perfectly inlaid Pt disk. Also, well-defined hemispherical Pt NPs with radii of 90 ± 30 nm were observed by scanning electron microscopy (SEM). Distinctly, we could measure a uniform height of ∼120 nm; however, various aspect ratios were seen (inset in Figure 4b), implying that Pt NPs spread out after reaching the steady state height during nucleation and growth.

DOI: 10.1021/acs.analchem.6b03024
Anal. Chem. 2016, 88, 10284−10289

Even with a well-defined tip and NPs confirmed by SEM, the shape of the Pt NPs was notably ellipsoidal in the SECM image (Figure 5a). Figure 5a shows this effect when H^+ is reduced to H_2 at the tip and the generated H_2 is reoxidized at a Pt NP with a 14 nm gap between the tip and apex of the NP. The image was obtained with a scan rate of 200 nm/s (20 nm incremental distance per 0.1 s incremental time, with a total image time of 88 s) at 134 nm constant height from HOPG substrate (more detailed information is in ref 24). Such an elongated shape of Pt NPs in SECM images is not reasonable based on the theoretical model of NP nucleation and growth[25,26] as well as our SEM observation in Figure 4b.

More importantly, the ellipsoidal geometry of NPs cannot successfully explain the observed electrochemical current over an individual NP in SECM images. From the SECM image, the NP dimensions with ellipsoidal geometry were extracted as 63 nm, 16 nm, 120 nm for the long axis radius, short axis radius, and height, respectively.[24] We theoretically predicted a tip current−distance curve over the NP as a function of the gap between the tip and apex of the NP under a mass transfer limited condition as presented in Figure 5b.[27]

This theoretical current−distance curve was compared to a curve with a hemispherical NP with a 63 nm radius and a 120 nm height. At a large gap (>100 nm) between the tip and apex of a NP, the theoretically predicted tip currents over each NP are similar under the mass transfer limit regardless of ellipsoidal or hemispherical geometries. However, as the tip approaches closer to a NP, i.e., a smaller gap between the tip and a NP, the difference in tip currents between different geometries of NPs becomes more prominent. At a 14 nm gap over the apex of a NP, where the SECM image in Figure 5a was obtained, a NP with ellipsoidal geometry displays obviously smaller currents than a hemispherically shaped NP.

In fact, the maximum current of cross-sectional responses along the red arrow in the SECM image (Figure 5a) matches well with that in the theoretical simulation using a hemispherical geometry as shown in Figure 5c, where the ET reaction at Pt NPs is controlled by diffusion. Note that there is a discrepancy in the current peak width between theoretical and experimental current profiles. This fitting result clearly indicates that a hemispherical geometry rather than an ellipsoidal geometry could explain the high activity of a Pt NP for the hydrogen oxidation reaction. Overall, considering all the aspects discussed above, it is likely that the ellipsoidal Pt NP in the SECM images could be an artifact. Then, why do we observe an ellipsoidal shaped NP in SECM image (Figure 5a) or a discrepancy in current peak width in Figure 5c? We speculate that the lockable micropositioner greatly helped to stabilize the tip position in the *z*-axis in the isothermal chamber, where the thermal drift was suppressed. This *z*-positional stability resulted in an SECM image that showed uniform background currents implying no discernible tip drift in the *z*-axis. In this regard, unlockable general micropositioners originally used in the *x* and *y*-axis could cause a serious drift or creeping in the lateral tip position when the piezo positioner scanned the tip, thereby distorting the SECM image in lateral direction. Such distorted images can also be seen in other SECM work, where unprecedentedly high spatial resolution images were introduced.[28] On the basis of this speculation, all micropositioners were replaced with lockable micropositioners. Consequently, we confirmed the spherical shape of the Pt NP in the SECM image studied with $FcTMA^+$ in Figure 6, where a tip oxidizes $FcTMA^+$ to $FcTMA^{2+}$ and the generated $FcTMA^{2+}$ is reduced back at the Pt NP as presented in Figure 4a (scan rate 200 nm/s; 20 nm incremental distance per 0.1 s incremental time; image time 420 s). The resulting image and the quantitative analysis indicate that unwanted tip drifts in the lateral direction could be successfully suppressed (more analysis is in the Supporting Information). More significantly, these results unambiguously prove that a single NP could be imaged by SECM.

CONCLUSIONS

In this work, we explicitly reported the crucial components including the software and the hardware to achieve nanoscale SECM. These findings enabled us to successfully build nanoscale SECM. Thus, in the previous work, we could propose that nanoscale SECM can be a useful approach to link the correlation between the structure and electrocatalytic activity of single nanostructures. For instance, it allows us to scrutinize the individual behavior of single NPs in a typical ensemble sample.

ASSOCIATED CONTENT

Supporting Information

The Supporting Information is available free of charge on the ACS Publications website at DOI: 10.1021/acs.analchem.6b03024.

Experimental conditions, overall operation and procedure of the instrumentation, and additional LabVIEW codes (both actual VI files and larger phase block diagram image files (generic version, so the users could use any manufacturer (PI, Newport, etc.) and just replace our "dummy" VIs with the manufacturer that they chose to use) (PDF)

Sample LabVIEW .vi files and larger images of the block diagrams (ZIP)

AUTHOR INFORMATION

Corresponding Authors

*E-mail: ajbard@mail.utexas.edu.

*E-mail: kcleonard@ku.edu.

Author Contributions

○J.K. and C.R. contributed equally to this work

Notes

The authors declare no competing financial interest.

ACKNOWLEDGMENTS

We acknowledge support of this research from the AFOSR MURI (FA9550-14-1-0003) and the Robert A. Welch Foundation (Grant F-0021). Also, the authors thank Tim Hooper (thooper@cm.utexas.edu) for the instrumental modification (Department of Chemistry and Biochemistry, The University of Texas at Austin).

REFERENCES

(1) Bard, A. J.; Mirkin, M. V. *Scanning Electrochemical Microscopy*, 2nd ed.; CRC Press, Boca Raton, FL, 2012.

(2) Shen, M.; Ishimatsu, R.; Kim, J.; Amemiya, S. *J. Am. Chem. Soc.* **2012**, *134*, 9856−9859.

(3) Kueng, A.; Kranz, C.; Lugstein, A.; Bertagnolli, E.; Mizaikoff, B. *Angew. Chem., Int. Ed.* **2003**, *42*, 3238−3240.

(4) Ueda, A.; et al. *Angew. Chem., Int. Ed.* **2007**, *46*, 8238−8241.

(5) Macpherson, J. V.; Unwin, P. R. *Anal. Chem.* **2000**, *72*, 276−285.

(6) Nagahara, L. A.; Thundat, T.; Lindsay, S. M. *Rev. Sci. Instrum.* **1989**, *60*, 3128.

(7) Kurulugama, R. T.; et al. *Anal. Chem.* **2005**, *77*, 1111−1117.

DOI: 10.1021/acs.analchem.6b03024
Anal. Chem. 2016, 88, 10284−10289

(8) Osbourn, D. M.; Sanger, R. H.; Smith, P. J. S. *Anal. Chem.* **2005**, *77*, 6999−7004.
(9) Zhao, X.; Diakowski, P. M.; Ding, Z. *Anal. Chem.* **2010**, *82*, 8371−8373.
(10) Pahler, M.; Santana, J. J.; Schuhmann, W.; Souto, R. M. *Chem. - Eur. J.* **2011**, *17*, 905−911.
(11) Lee, Y.; Ding, Z. F.; Bard, A. J. *Anal. Chem.* **2002**, *74*, 3634−3643.
(12) Hengstenberg, A.; Blochl, A.; Dietzel, I. D.; Schuhmann, W. *Angew. Chem., Int. Ed.* **2001**, *40*, 905−908.
(13) Takahashi, Y.; Shiku, H.; Murata, T.; Yasukawa, T.; Matsue, T. *Anal. Chem.* **2009**, *81*, 9674−9681.
(14) Nebel, M.; Eckhard, K.; Erichsen, T.; Schulte, A.; Schuhmann, W. *Anal. Chem.* **2010**, *82*, 7842−7848.
(15) Takahashi, Y.; et al. *J. Am. Chem. Soc.* **2010**, *132*, 10118−10126.
(16) Comstock, D. J.; Elam, J. W.; Pellin, M. J.; Hersam, M. C. *Anal. Chem.* **2010**, *82*, 1270−1276.
(17) Takahashi, Y.; et al. *Angew. Chem., Int. Ed.* **2011**, *50*, 9638−9642.
(18) Ebejer, N.; Schnippering, M.; Colburn, A. W.; Edwards, M. A.; Unwin, P. R. *Anal. Chem.* **2010**, *82*, 9141−9145.
(19) Takahashi, Y.; Schevchuk, A. I.; Novak, P.; Babakinejad, B.; Macpherson, J.; Unwin, P. R.; Shiku, H.; Gorelik, J.; Kienerman, D.; Korvchev, Y. E.; Matsue, T. *Proc. Natl. Acad. Sci. U. S. A.* **2012**, *109*, 11540−11545.
(20) Nioradze, N.; Chen, R.; Kim, J.; Shen, M.; Santhosh, P.; Amemiya, S. *Anal. Chem.* **2013**, *85*, 6198−6202.
(21) Nioradze, N.; Chen, R.; Kurapati, N.; Khcataeva-Domanov, A.; Mabic, S.; Amemiya, S. *Anal. Chem.* **2015**, *87*, 4836−4843.
(22) Kim, J.; Shen, M.; Nioradze, N.; Amemiya, S. *Anal. Chem.* **2012**, *84*, 3489−3492.
(23) Barforoush, J. M.; McDonald, T. D.; Desai, T.; Widrig, D.; Bayer, C.; Brown, M. K.; Cummings, L. C.; Leonard, K. C. *Electrochim. Acta* **2016**, *190*, 713−719.
(24) Kim, J.; Renault, C.; Arroyo-Currás, N.; Nioradze, N.; Leonard, K. C.; Bard, A. J. *J. Am. Chem. Soc.* **2016**, *138*, 8560−8568.
(25) Gunawardena, G.; Hills, G.; Montenegro, I.; Scharifker, B. *J. Electroanal. Chem. Interfacial Electrochem.* **1982**, *138*, 225−239.
(26) Fleischmann, M.; Thirsk, H. R. *Advances in Electrochemistry and Electrochemical Engineering*, Vol. 3; Interscience: New York, 1963; Chapter 3.
(27) Yu, Y.; Sun, T.; Mirkin, M. V. *Anal. Chem.* **2015**, *87*, 7446−7453.
(28) Sun, T.; Yu, Y.; Zacher, B. J.; Mirkin, M. V. *Angew. Chem., Int. Ed.* **2014**, *53*, 14120−141.

DOI: 10.1021/acs.analchem.6b03024
Anal. Chem. 2016, 88, 10284−10289